Investigation of the Effect of Gradual Change of the Inner Tube Geometrical Configuration on the Thermal Performance of the Double-Pipe Heat Exchanger

Ahmadi, Nima**+; Ashrafi, Hojjat; Rostami, Sadra; Vatankhah Reza
Department of Mechanical Engineering, Technical and Vocational University (TVU), Tehran, I.R. IRAN

ABSTRACT: *Today, with the development of technology, heat transfer, reducing the time of heat transfer, reducing the size of heat exchangers, and increasing the efficiency are considered. Heat exchangers have many applications in the industry. Therefore, increasing the efficiency of heat exchangers will increase the overall efficiency of a system and optimize energy consumption by a system. In the present study, the main goal is the study the effects of the gradual changes in the inner tube geometrical configuration on the thermal performance of the double-pipe heat exchanger on the thermal performance using Computational Fluid Dynamics (CFD) methods based on the finite volume method. For validation, the results are compared with the valid results previously presented in the published papers, and there is a very good agreement between them. In addition to the basic model, six different geometrical designs are used for the inner tube, in the form of a flat tube and a nozzle-like tube. After the numerical simulation, the increase in heat transfer and the Nusselt number of flow, pressure drop, thermal efficiency, and the performance index were calculated for each model and compared with the base model and other models. The results show that the nozzle-like inner tube model has a lower performance than the base model. The model with a flat inner tube, and especially case 4 (The case with the flat inner tube with the aspect ratio of 0.3), has a very impressive performance compared to the base case at Reynolds numbers below 6000. But at higher Reynolds numbers, the basic model will have better overall conditions.*

KEYWORDS: *Double-pipe heat exchanger; Convection; CFD; Performance; Nusselt number; Nozzle-like tube.*

INTRODUCTION

Heat exchangers have many applications. These applications include power plants, refineries, petrochemical industries, manufacturing industries, food and pharmaceutical industries, metal smelting industries, heating, air conditioning, refrigeration systems, and space applications. Heat exchangers are widely used in various devices such as boilers, condensers, evaporators, cooling towers, preheaters, fan coils, oil coolers and heaters, radiators, furnaces, etc.

**To whom correspondence should be addressed.*
+ E-mail: nima.ahmadi.eng@gmail.com
1021-9986/2023/7/2305-2317 13/$/6.03

For this reason, the design of heat exchangers is very important[1]. The high efficiency of heat exchangers significantly contributes to overall energy and cost savings. Therefore, improving the performance of double-pipe heat exchangers is very important [2].

Liao and *Xin* [3], used the perforated tape twisted inside the circular tube to improve the heat transfer from the tube wall. *Chen et al*.[4] used indentations on the inner tube to improve heat transfer. *Eiamsa et al*. [5] continued the work of Liao and Xin and used the perforated tape twisted inside the circular tube to improve the heat transfer from the tube wall. They used different arrangements for twisted perforated tape. *Nagarani et al*.[6] used circular and elliptical annular fins to improve heat transfer in a double-pipe exchanger and observed that the performance of elliptical fins is better than circular fins and the efficiency of the fin is higher in elliptical mode. *Iqbal et al*.[7] investigated the optimal shape of parabolic, triangular and trapezoidal vanes using finite element numerical method and genetic algorithm and concluded that none of the vanes alone can be used in all modes and conditions be optimal. *Khanan et al.* [8] studied heat transfer in a two-tube exchanger with annular fins. Finally, the performance of annular vanes was evaluated better than others. *Zhang et al*.[9] experimentally studied the heat transfer in a two-tube heat exchanger using spiral fins and measured the velocities using the LDA method. *Bhuiya et al*. [10] continued the work of Liao and *Eiamsa et al*. *Totala et al*.[11] conducted experiments on a two-tube heat exchanger with threads inside the inner tube and observed a significant increase in heat transfer and Nusselt number compared to the condition without threads. But the required pumping power also increased compared to the case without thread. *Karanth et al*. [12] performed a numerical and experimental study of heat transfer in a double-tube heat exchanger and the effect of fins created on the outer wall of the inner tube of different geometric shapes, including rectangular, triangular and parabolic, on heat transfer in the heat exchanger. They did the results show that the performance of rectangular vanes is better compared to other vanes. *Ahmadi et al.* [13] investigated the effect of the thermos- exergitic behaviour of a corrugated heat exchanger with a two-phase flow. They observed a maximum increment of %32 was observed at Exergy destruction.

In this research, the thermal performance of double-tube exchangers is investigated and studied by changing the internal geometry to a flat tube and a nozzle-like tube, using numerical methods that are relatively low-cost methods. The innovation in this study is to investigate the thermal performance of the double-tube heat exchanger for different dimensions of the inner flat tube and inner nozzle tube. The heat transfer coefficient, pressure drop, Nusselt number, performance index and thermal efficiency will be calculated for each case and compared to other cases.

THEORETICAL SECTION

Problem statement

For the present study, the geometries of the double-tube heat exchanger in 7 different modes have been considered. For cases, 1 to 4, (case 1 is the same as the base case) the areas and dimensions of the internal and external pipes are constant throughout the converter and there is no difference between the inlet and outlet. The geometry of the inlet for different modes from 1 to 4 (modes 2 to 4 are with a flat inner tube) is compared with the details in Fig.1. The length of the converter is 500 mm in all modes.

for different states of the aspect ratio (*Ar*) which is calculated by the following relationship, where *W* is the width of the inlet section of the internal flat pipe and *B* is the length of the inlet section.

$$Ar = \frac{W}{W + B}$$

For cases 5 to 7, a nozzle-like geometry is used for the inner pipe, but the diameter of the outer pipe is fixed, and the area of the inlet and outlet of the pipes has been changed. Fig. 2 and Table 1 show the geometrical specifications for cases with a nozzle-like inner tube.

In all cases, the heat exchanger is a heat exchanger with the counter flow, which is shown in Fig. 3 for the entry and exit directions of cold and hot fluid.

Governing equations

The flow studied in this research is as Table, incompressible flow and the change in fluid properties due to temperature change is ignored. Therefore, the equations governing the Table 2.

Definition of performance indicators

In the heat exchanger, several hydrodynamic and thermal index parameters determine the performance of a heat exchanger as shown in Table 3 [14, 15].

Table 1: Geometric specifications of inlet and outlet diameters

Case	L (Length)	$D_{h,o}$	$D_{h,i}$
Case 5	500mm	20mm	25mm
Case 6	500mm	16mm	25mm
Case7	500mm	12mm	25mm

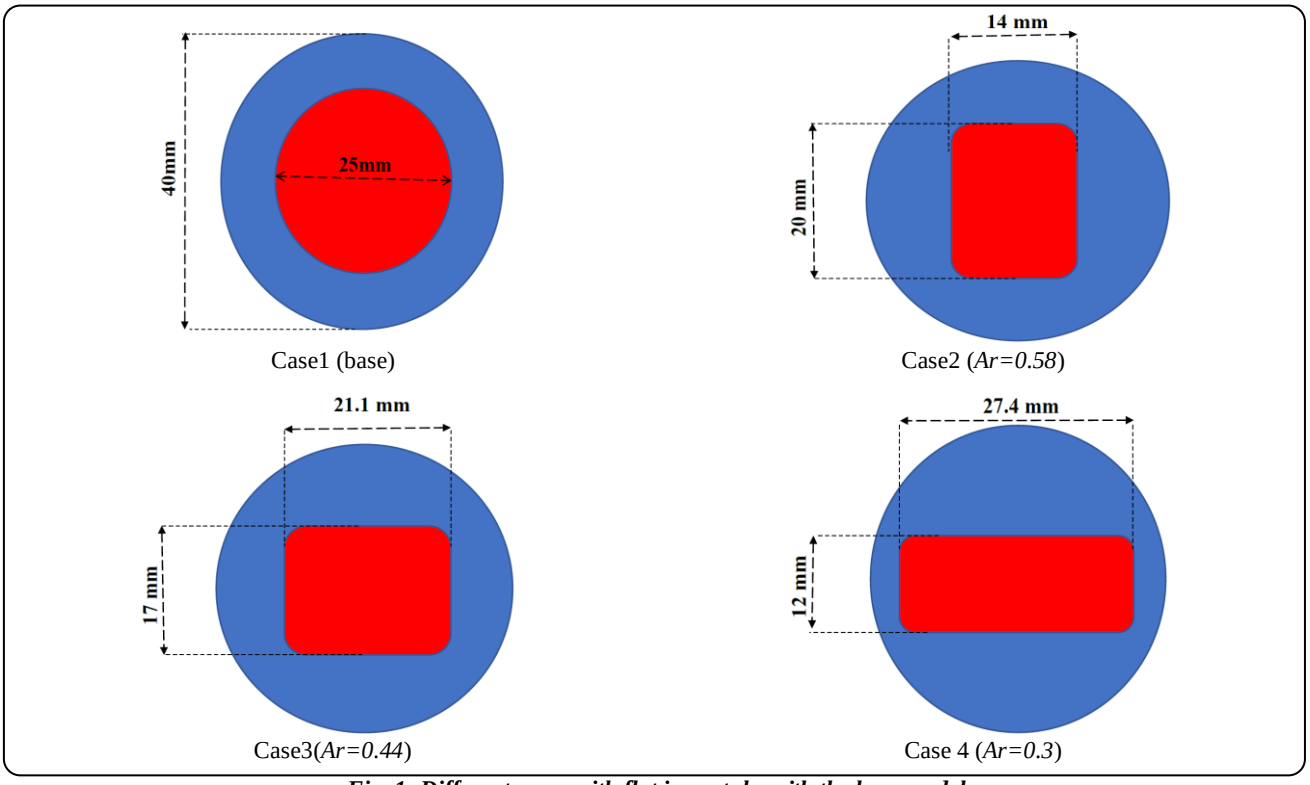

Fig. 1: Different cases with flat inner tube with the base model

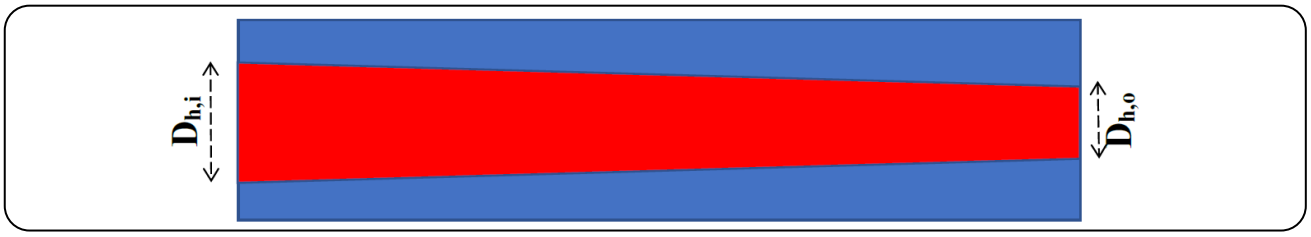

Fig. 2: The side view of cases 5 to 7

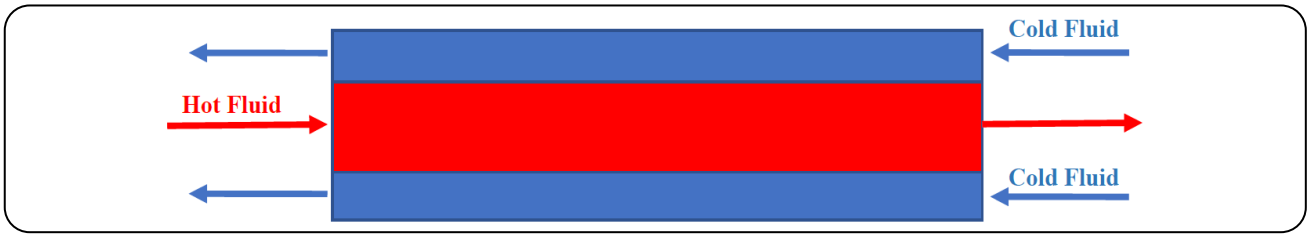

Fig. 3: the entry and exit directions of cold and hot fluid

Table 2: Governing equations

Continuity	$\nabla \cdot V = 0$	(1)	V: fluid velocity
Momentum	$\nabla \cdot (\rho VV) = -\nabla P + \nabla \cdot \left((\mu + \mu_t)\nabla V\right) + \nabla \cdot \left(-\rho\overline{V'V'}\right)$	(2)	ρ: density, P: pressure, μ: dynamic viscosity, μ_t: turbulence viscosity, V': velocity fluctuations.
Energy	$\rho C_p V \cdot \nabla T = \nabla \cdot \left(k_{eff}\nabla T\right)$	(3)	T : temperature Cp : heat capacity k_{eff}: effective conductivity coefficient
Realizable k-e	$\nabla \cdot (\rho Vk) = \nabla \cdot \left(\left(\mu + \frac{\mu_t}{\sigma_k}\right)\nabla k\right) + G_k + G_b - \rho\varepsilon - Y_M$	(4)	$C_1 = max\left(0.43, \frac{\eta}{\eta+5}\right)$ $\eta = S\frac{k}{\varepsilon}$ $S = \sqrt{2S_{ij}S_{ij}}$ $S_{ij} = \frac{1}{2}\left(\frac{\partial u_j}{\partial x_i} + \frac{\partial u_i}{\partial x_j}\right)$
	$\nabla \cdot (\rho V\varepsilon) = \nabla \cdot \left(\left(\mu + \frac{\mu_t}{\sigma_\varepsilon}\right)\nabla\varepsilon\right) + \rho C_1 S\varepsilon - \rho C_2 \frac{\varepsilon^2}{k+\sqrt{v\varepsilon}} + C_{1\varepsilon}\frac{\varepsilon}{k}C_{3\varepsilon}G_b$	(5)	

Table 3: Definition of performance indicators

The heat is transferred from the hot fluid in the inner tube and the cold fluid in the outer tube	$Q_h = \dot{m}_h c_{p,h}(T_{in} - T_{out})_h$	(6)
	$Q_c = \dot{m}_c c_{p,c}(T_{in} - T_{out})_c$	(7)
Mean heat transfer	$Q = \left(\frac{Q_h + Q_c}{2}\right)$	(8)
The ratio between actual and maximum achievable heat transfer rates represents the effectiveness	$\gamma = \left(\frac{Q}{Q_{max}}()\right)$	(9)
	$Q\left(\dot{m}c_p\right)\left(T_{h,in} - T_{c,out}\right)_{min\,max}$	(10)
Overall convective heat transfer coefficient	$\tilde{U} = \frac{Q}{A_i \Delta T_{LMTD}}$	(11)
	$\Delta T_{LMTD} = \frac{\Delta T_1 - \Delta T_2}{ln\left(\frac{\Delta T_1}{\Delta T_2}\right)}$	(12)
	$\Delta T_1 = T_{h,in} - T_{c,out}$, $\Delta T_2 = T_{h,out} - T_{c,in}$	
Mean convective heat transfer coefficients on the inner pipe and annulus	$\overline{h_{pipe}} = \frac{-\overline{q_w''}}{0.5\left(T_{h,in} + T_{h,out}\right) - \overline{T_w}}$	(13)
	$\overline{h_{annulus}} = \frac{-\overline{q_w''}}{\overline{T_w} - 0.5\left(T_{c,in} + T_{c,out}\right)}$	(14)
mean Nusselt numbers in the inner pipe and annulus	$\overline{Nu_{pipe}} = \frac{\overline{h_{pipe}}D_{h,pipe}}{k_c}$	(15)
	$\overline{Nu_{annulus}} = \frac{\overline{h_{annulus}}D_{h,annulus}}{k_c}$	(16)
Friction coefficient on the inner pipe and annulus side	$f_i = \frac{\Delta P_i}{\frac{1}{2}\rho V_{i,pipe}^2 \frac{L}{D_{h,pipe}}}$	(17)
	$f_o = \frac{\Delta P_o}{\frac{1}{2}\rho V_{i,annulus}^2 \frac{L}{D_{h,annulus}}}$	(18)
The ratio of overall heat transfer rate to total pressure drop: heat exchanger performance index. Also, the total pressure drop is the summation of the pressure drop in the inner tube plus the pressure drop in the outer tube.	$\eta = \frac{Q}{\Delta P_{tot}}$ $\Delta P_{tot} = \Delta P_i + \Delta P_o$	(19)
Reynolds numbers on the inner pipe side and annulus side	$Re_{pipe} = \frac{(\rho V_i D_h)_{pipe}}{\mu_h}$	(20)
	$Re_{annulus} = \frac{(\rho V_i D_h)_{annulus}}{\mu_c}$	(21)

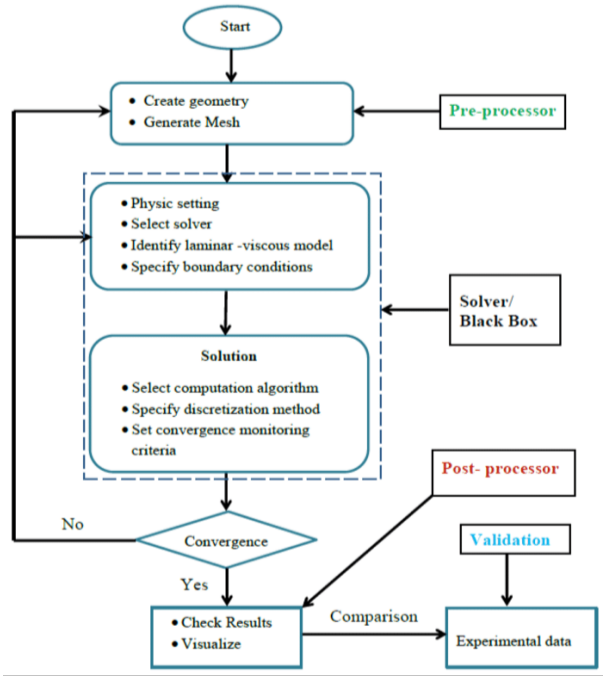

Fig. 4: Flowchart of the solution procedure

Boundary conditions and solution method

The hot fluid in this study is water entering the inner tube at a temperature of 60 °C (333 K) at an inlet velocity calculated by the following equation and varying for different Reynolds numbers. Turbulence intensity and hydraulic diameter for fluid turbulence calculations were calculated using the following equation [16]:

$$V_{i,pipe} = \left(\frac{Re \times \mu}{\rho D_h}\right)_{pipe}, v = w = 0 \qquad T = 333K, I = 16\,Re^{-0.125} \tag{22}$$

In the outer tube, the cold fluid enters the outer tube with a constant mass flow rate of 0.1 kg/s for all modes and with a temperature of 20 degrees Celsius (293 K) against the direction of the hot fluid flow. The fluid velocity is calculated as follows:

$$V_{i,annulus} = \frac{\dot{m}_c}{\rho A_o}, v = w = 0 \qquad T = 293K, I = 16\,Re^{-0.125} \tag{23}$$

At the outlet of the pipes, the boundary condition of the outlet pressure is equal to the atmospheric pressure used. For cases where the outlet diameter is equal to the inlet diameter, the same turbulence intensity and hydraulic diameter are used. For the wall boundary condition, a no-slip condition is considered for the fluid in contact with all

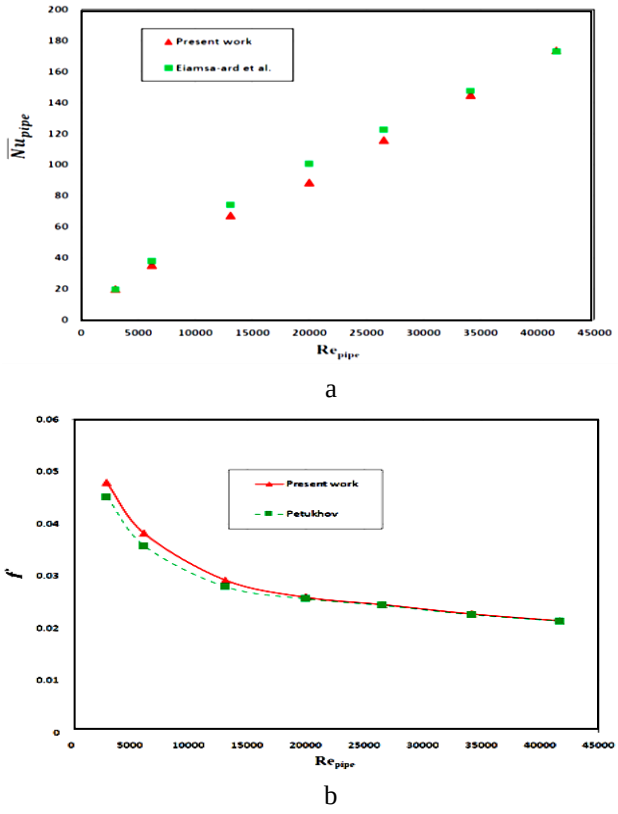

Fig. 5: Validation of the model for the average Nusselt number (a) and the friction coefficient (b) in the inner tube wall

the walls of the exchanger. The thermal insulation boundary condition (zero heat flux) is used on the outer wall of the outer tube. The pressure drop in a tube can be indicated by [17]:

$$\Delta P = f_i \frac{L}{D_h} \frac{\rho V^2{}_{i,pipe}}{2} \tag{24}$$

The numerical solution flowchart for the present study is presented in Fig. 4.

RESULTS AND DISCUSSION

At first, the simulation results were compared with the results published in reliable journals to validate and check the independence of the grid for the base case (Case 1). As seen in Fig. 5a, 5b, the validation results for the base model (Case1) compared with the published results of *Eiamsa et al.* [5] for the Nusselt number and the results of the work of *Petukhov et al.* [17] for the friction coefficient. The results indicate that there is a very good agreement between the simulation results of the present work and

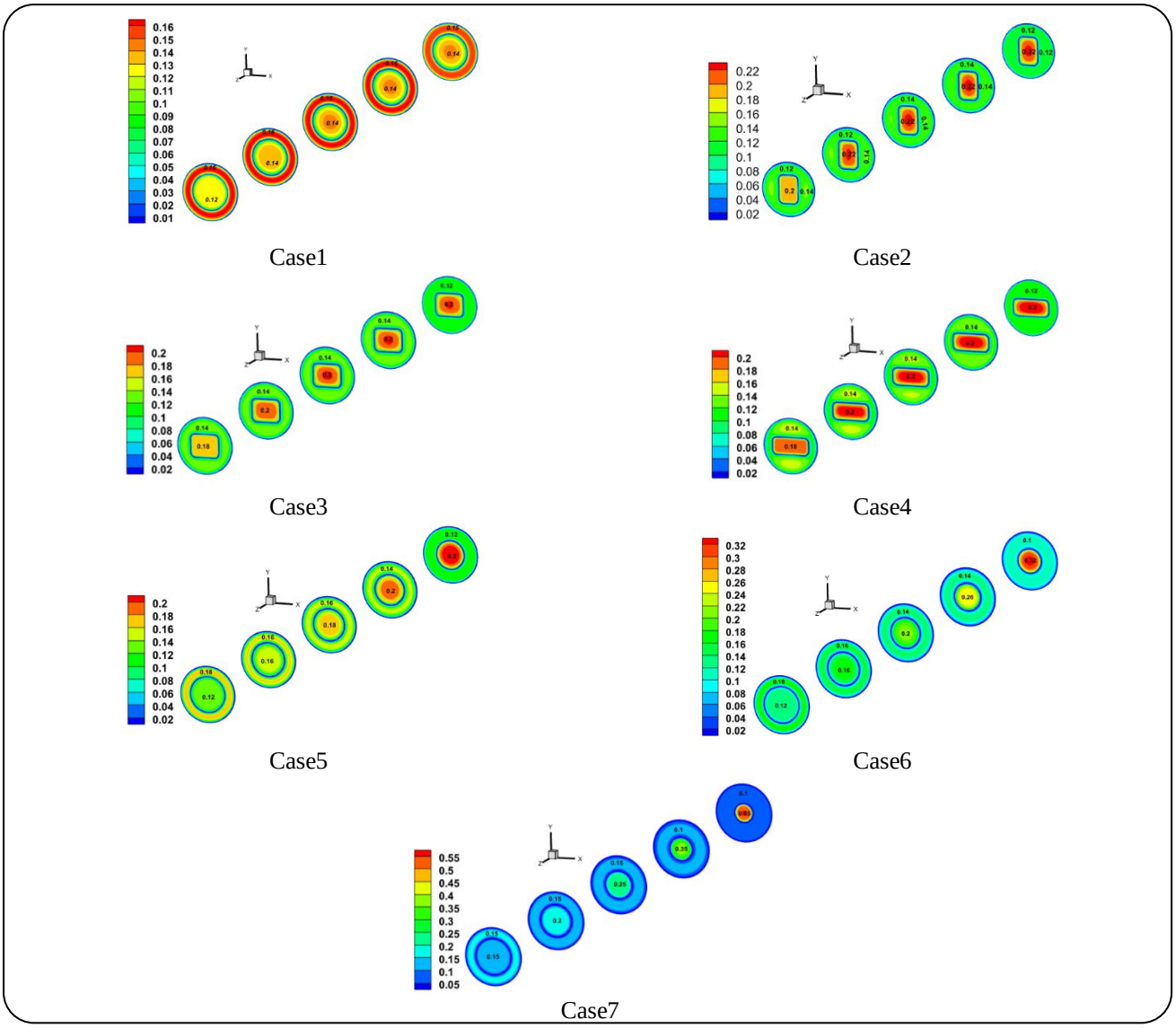

Fig. 6: Comparison of flow velocity distribution for different cases

the mentioned results. Therefore, the model created for the next states and checking the geometrical effects will be correct and reliable.

Solving the equations governing the fluid field has been done using the finite volume method [17, 18]. SIMPLE algorithm [18] is used for velocity and pressure coupling. The displacement term of the equations of momentum, energy, turbulence kinetic energy and turbulence energy loss are discretized using the second-order upwind method [18, 19]. The pressure gradient term is discretized using a second-order approximation. An 8-core computer with 8 GB of RAM was used to solve the problem. Each mode simulated at Reynolds numbers of 3000, 6000, 13000, 20000, 26000, 34000 and 41000. The average time for (which includes 49 modes) the simulation of each mode at each Reynolds number is about 8 hours [20].

To study the effect of geometric conditions on the performance of the heat exchanger, the results of cases 1 to 7 are compared, and the results of the simulation of these cases and their comparison with the basic model and with each other are presented below.

Velocity distribution

Fig. 6 shows the velocity distribution for different modes from 1 to 4 at Reynolds number 6000 for different modes. By reducing the area and according to Eqs (22) and (23), the velocity in the inner tube will increase.

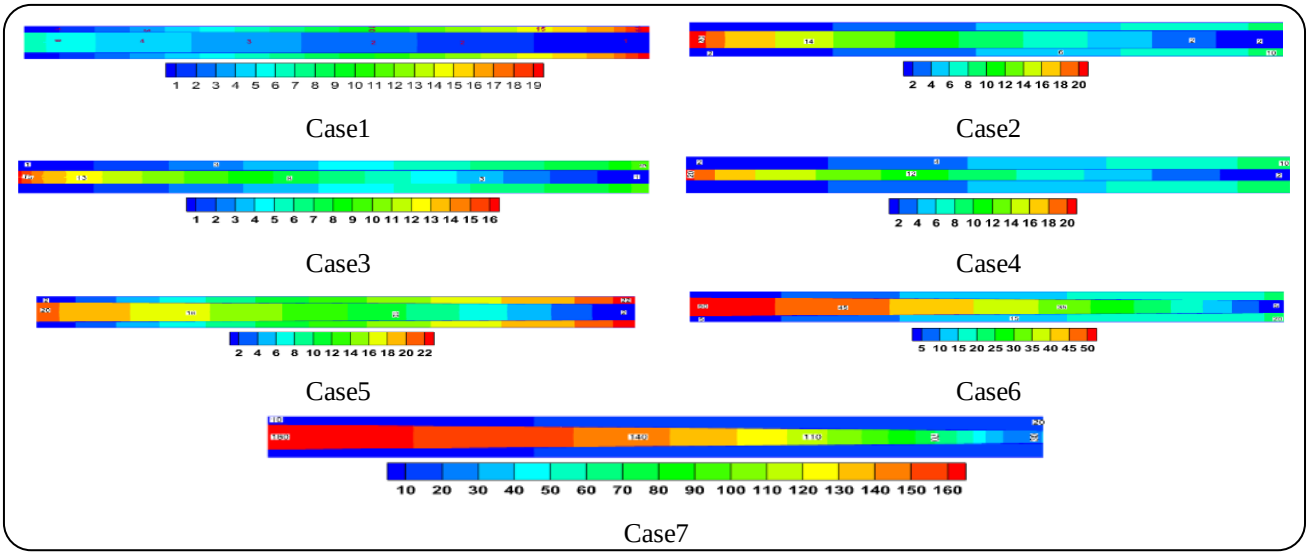

Fig. 7: Comparison of pressure drop for different cases

By reducing the cross-section of the inner tube, it can be seen that the length of the inlet in the inner tube has increased and the flow has reached the developed state later.

In the outer pipe, it is completely the opposite, as the cross-section of the inner pipe decreases, and as a result, the flow rate decreases slightly with the increase of the cross-section of the outer pipe. For this reason, in the case of flat pipe (Cases 2 to 4), the greatest increase in speed is related to Case 2, and a slight decrease in speed is also observed in the external channel. But in the case of the nozzle-like tube (Cases 5 to 7), considering that the lowest cross-sectional area of the channel is related to Case 7, the greatest increase in speed in the inner tube and decrease in speed in the outer tube are also related to this case. The development of fluid flow in this case also happened much later than in other cases.

Pressure drop

Fig. 7 shows the pressure drop distribution for cases 1 to 7 at Reynolds 6000. For better comparison, the Figs. are shown from the side view of the heat exchanger, where the shape of the inner and outer tubes is visible.

The pressure drop will increase with the reduction of the inlet cross section (Figs. 7 and 8a). In the case of the flat inner tube, Case 2 has the highest-pressure drop and in the case of the nozzle-like inner tube, case 7 has the highest-pressure drop. Overall, Case 7 has the highest-pressure drop among all cases.

Considering that the heat exchanger has opposite flow in all cases, the hot fluid flow is entered from the opposite direction, in other words, the coordinate origin is at the beginning of the external pipe inlet and the hot fluid flow is entered from the end of the pipe (for example, in Fig. 8a). The fluid flow in the Figure is not from the origin, but at the end of 0.5 meters, and the end of the outlet is at the origin of coordinates.

Fig. 8b shows the pressure drop in the outer pipe. Case 2 has the lowest pressure drop in the outer pipe for the flat pipe condition. Due to the increase of the hydraulic diameter and the increase of the cross-section, the amount of pressure drop and friction in the channel will decrease. But in cases related to the nozzle-shaped inner tube, the pressure drop analysis is different. Since in nozzle-like cases, the inlet dimensions are the same, but the reduction of the inner tube diameter is faster in Case 7, so the flow is developed later and in Case 5, this amount is less. The later development makes the pressure drop in the nozzle-shaped tube lower in Case 7 and higher in Case 5. However, as the flow advances, considering that the internal channel diameter decreases faster in Case 7, it can be seen that the pressure drop in the last half of the channel is higher than in the other two cases. Fig. 9 shows the overall pressure drop in heat exchangers at different Reynolds numbers (Reynolds numbers 3000, 6000, 13000 and 20000). It can be seen that in all cases, the pressure drop increases with the increase of the Reynolds number. But Case 7 shows the highest overall pressure drop.

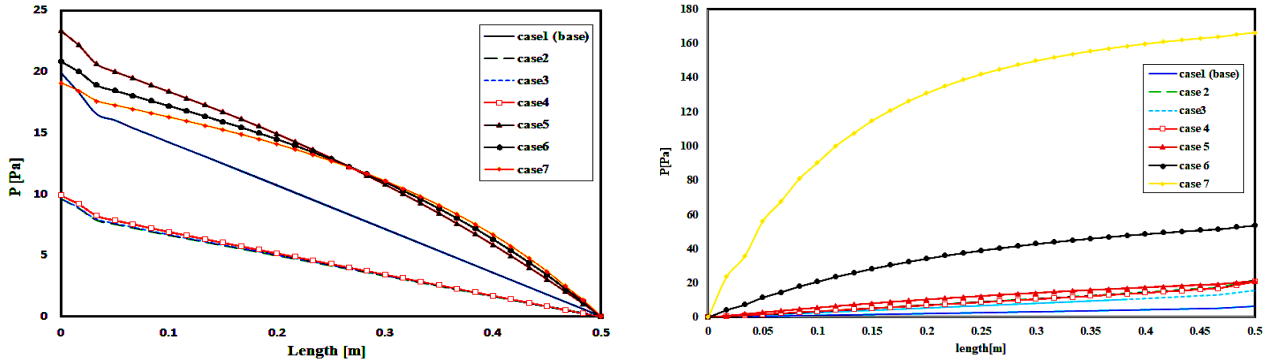

b a

Fig. 8: Pressure drop in the inner tube (a) and in the external tube (b) for all cases

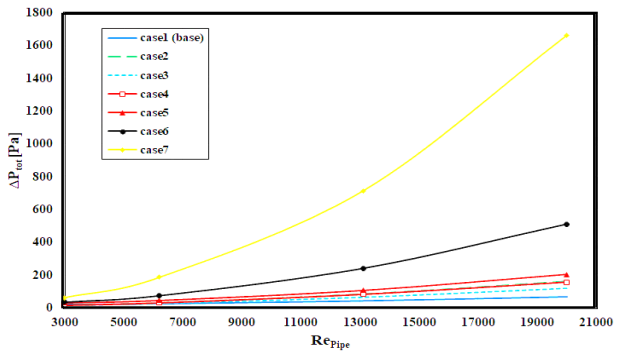

Fig. 9: Total pressure drops for all cases at different Reynolds numbers

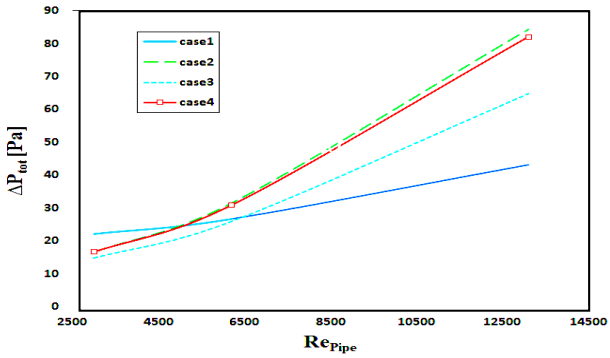

Fig. 10: Total pressure drop for cases 1 to 4 at low Reynolds numbers

To discuss the overall pressure drop in the case of a flat inner tube, special attention needs to be paid to Reynolds numbers below 6000, given that this is not evident in Fig. 9. As indicated in eq. 24, the pressure drop is increased along the tube and by increasing the velocity. As it is clear, Case 7 has the maximum velocity magnitude so that it experiences the maximum pressure drop in the longitudinal direction due to the maximum pressure drop in the inner pipe. Therefore, Fig. 10 clearly shows the total pressure drop for cases 1 to 4 at low Reynolds numbers. According to Fig. 10, it can be seen that at Reynolds numbers lower than 6000, the amount of pressure drop is generally different. In this period, as can be seen, the pressure drop in all cases with a flat inner tube is lower than the base case, which is the lowest pressure drop for Case 3. For example, the percentage of reduction in pressure drop, in Reynolds number 3000, for modes 2 to 4 compared to mode 1 is 25.1%, 32.6% and 23.5% respectively. But with the increase of Reynolds number to numbers above 6000, the amount of pressure drop in cases with flat inner tubes increases, so for example, for Case 3 at Reynolds number 13000, the increase in pressure drop compared to Case 1 is 33.2%. The reason for this is that, at low Reynolds numbers, the decrease in pressure drop in the outer tube reduces the increase in total pressure drop, but at high Reynolds numbers, the increase in pressure in the inner tube overcomes this and the total pressure drop increases.

Temperature distribution

Fig. 11 shows the temperature distribution in the lateral cross-section of the heat exchanger for all cases at a Reynolds number of 6000. The labels on each point easily indicate the temperature of each case.

Fig.12 show the temperature distribution diagram in the inner and outer tubes for all cases at Reynolds number 6000. According to these Figs., it can be seen that in flat inner tube cases, the temperature in the inner tube at the end of the tube has dropped more than the base state. On the contrary, the temperature in the outer tube is higher in these cases, which indicates that the inner tube of the bed has caused better heat transfer from the hot fluid to the cold fluid in the outer tube. The highest heat transfer is in Case 2.

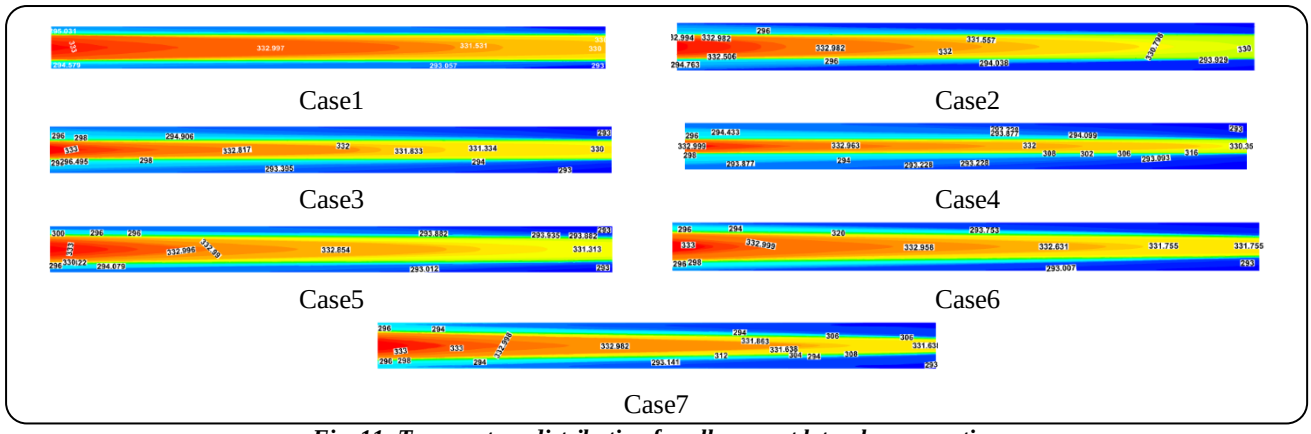

Fig. 11: Temperature distribution for all cases at lateral cross-section

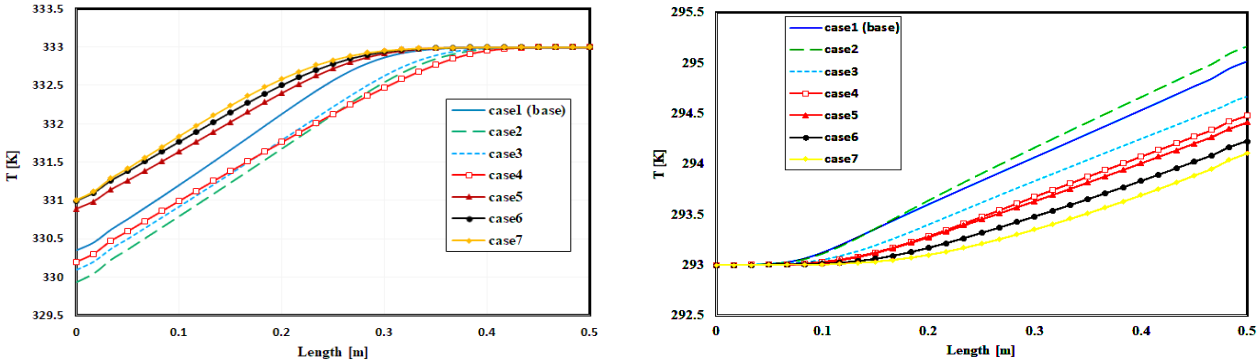

Fig. 12: Temperature distribution in the inner tube (a) and in the outer tube (b) at Reynolds number 6000

The cases related to the nozzle-like tube also have a weaker performance in this matter than the basic case, which is the lowest heat transfer rate related to Case 7 of these cases. In the case of a nozzle-like pipe, due to the increase in the flow rate, the fluid flow does not have enough time during the heat exchanger to transfer heat, and therefore the fluid flow in these cases has a lower heat loss along the channel. Also, due to the reduction of the heat transfer area during the flow, the heat transfer in these modes is lower than in the base model. Case 2 transfers heat to the outer channel in a more appropriate way due to the larger area in the flow path.

Convective Heat transfer

In Fig. 13a, it can be seen that the average convection heat transfer coefficient and the average Nusselt number inside the inner tube increase in most cases with the increase of the Reynolds number. In most of these cases and especially in low Reynolds numbers (Reynolds lower than 13000), this increasing behaviour has an almost linear form. In Reynolds numbers smaller than 7000 for all cases, the average convection coefficient and average Nusselt number are higher than the base case. But with the increase of the Reynolds number, it can be seen that for the basic state, the rate of growth of the average heat transfer coefficient and average Nusselt number has happened at a faster rate. However, the highest value is for Case 7. Creating a flat tube inside the heat exchanger and consequently reducing the area of the flow entrance in it by reducing the aspect ratio, increases the speed and consequently the convection power of the flow (as can be seen in Reynolds numbers lower than 7000 in Fig. 13a). With the increase of the Reynolds number and with the increase of the pressure drop in the inner tube in the case of the flat inner tube (when the aspect ratio is reduced), it is clear that the heat transfer coefficient decreases. But in the case of the nozzle-shaped tube, the excessive increase in the flow rate, especially in Case 7, will increase the average coefficient of convection heat transfer.

According to Fig. 13b, we find that in different Reynolds numbers, sometimes the average Nusselt number acts independently of the average convection heat

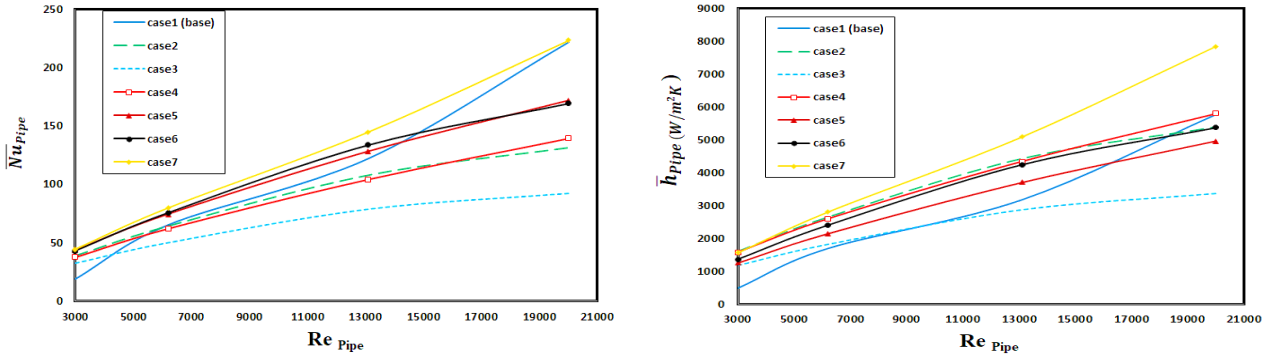

b a

Fig. 13: Average convection heat transfer coefficient (a) and the average Nusselt number (b) in the inner tube

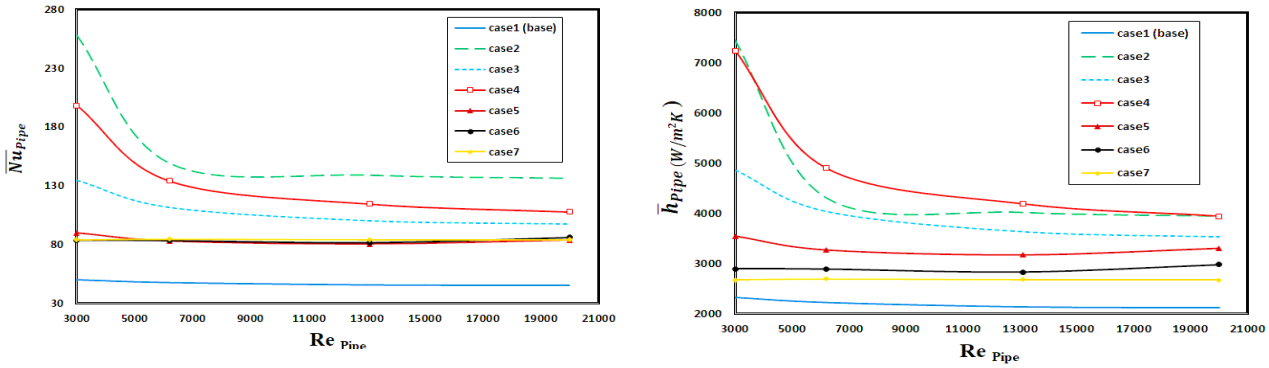

b a

Fig. 14: Average convection heat transfer coefficient (a) and the average Nusselt number (b) in the outer tube

transfer coefficient, which is due to the effect of the hydraulic diameter on the average Nusselt number (Equation 15). Thus, with the reduction of the inlet area, the hydraulic diameter is also reduced, which can compensate for the reduction of the area and keep the Nusselt number constant, and even do the complete opposite and reverse the effect of increasing the average convection coefficient.

According to Figs. 14a, and 14b, it is visible that the average convection heat transfer coefficient and the average Nusselt number, in the outer tube, decrease with the increase of the Reynolds number in almost all geometric modes. This is because the increase in the Reynolds number in the inner tube will reduce the convection heat transfer power of the cold fluid in the outer tube, which itself causes the temperature difference between the hot fluid and the inner wall to decrease. Therefore, the temperature in the inner wall increases. As a result, the temperature difference between the cold fluid in the outer tube and the temperature of the inner wall increases with the increase of the Reynolds number, which will decrease the convection heat transfer coefficient in the outer tube.

The average convection heat transfer coefficient and the average Nusselt number for all geometric modes and all Reynolds numbers in the outer tube are higher than the base model (Fig. 14b). But the value of the average convection coefficient is the highest for Case 4 and Case 2, and the average Nusselt number is the highest for Case 2 and Case 4. That is, the average convection heat transfer coefficient has the highest value at Ar=0.3, which happens for low Reynolds and around 3000, at Ar=0.5. But the Nusselt number has the maximum value in all Reynolds at Ar=0.5 (Case 2). The fact that in cases 2 and 4, the convection coefficient and the Nusselt number are the opposite of each other is that the hydraulic diameter decreases with the reduction of the aspect ratio, which affects the reduction of the aspect ratio.

Fig. 15 shows the comparison of the overall convection heat transfer coefficient between different cases per Reynolds number. In all cases, with the increase of the Reynolds number, the amount of this coefficient has also

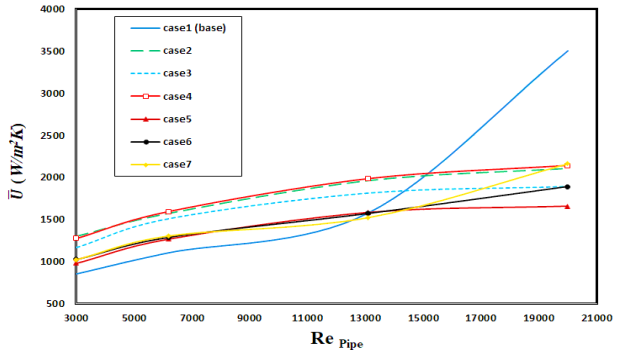

Fig. 15: Overall heat transfer coefficient for different Reynolds numbers

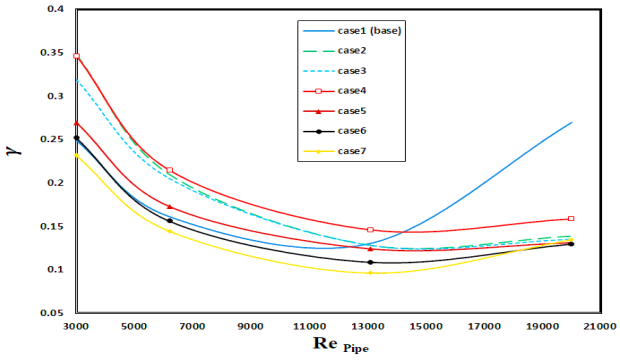

a

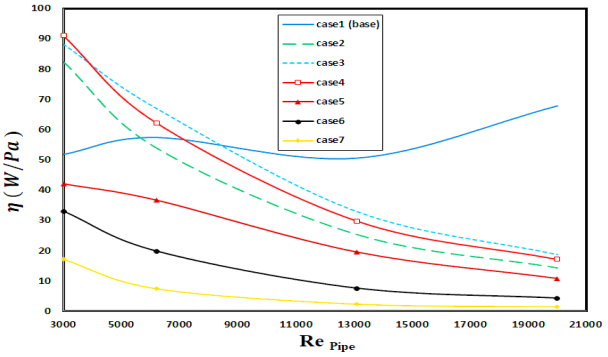

b

Fig. 16: The coefficient of thermal efficiency (a) and the Performance index coefficient (b)

increased. It should be noted that in the low Reynolds range, below 4000, Case 2 has the highest coefficient. But at higher Reynolds, its value is slightly higher for Case 4. For Reynolds above 15,000, the overall convection coefficient for the base model (Case1) is higher than all the geometric modes. For higher Reynolds, Case 7 will also see a large increase in the overall convection heat transfer coefficient. For example, in Reynolds number 6000, the percentage increase of this coefficient for modes 2 to 7 is 29.7%, 26.8%, 30.6%, 12.6%, 14.6% and 15.3% respectively.

Fig. 16a shows the thermal efficiency of the heat exchanger per Reynolds number for all geometric cases. This coefficient almost decreases with the increase of Reynolds number up to 13000 Reynolds number. Fig. 16b compares the performance index of the two-pipe converter for different cases for increasing the Reynolds number. According to the Fig., it is clear that the amount of this index decreases with the increase of the Reynolds number in all modes except the base model. In Reynolds numbers lower than 4000, the value of this index is the maximum value for mode 4. With the increase of the Reynolds number, due to the increase of the pressure drop in mode 4, the performance index coefficient will experience a greater drop. At Reynolds numbers below 6000, this coefficient is higher than the base case in the case of the flat inner tube and lower than in the case of the nozzle-shaped tube. By increasing the Reynolds number to more than 9000, due to the strong increase in the overall pressure drop in flat tube conditions and the low increase in overall heat transfer in the exchanger, the performance index coefficient in the flat inner tube conditions will drop to lower values than the base condition. In case 7, due to less heat transfer and high-pressure drop, this coefficient is the lowest.

Fig. 17 shows the friction coefficient for the outer and inner pipe, respectively, for different cases. The use of the inner flat tube has reduced the friction coefficient for the outer tube for case 3 by a very small amount compared to the base model. As can be seen from equation 18, the amount of friction coefficient in the outer pipe has a direct relationship with the pressure drop and hydraulic diameter and inversely with the square of the speed. According to these indicators, the use of an internal converging tube increases this coefficient significantly. But the use of the flat inner tube and especially in case 3 has slightly reduced this coefficient. In Fig. 17b, the coefficient of friction for the inner tube is compared with each other for different Reynolds numbers. According to equation 17, which calculates the friction coefficient of the inner tube, and according to Fig. 17b, it can be seen that the use of a flat inner tube has slightly reduced the friction coefficient in the inner tube compared to the base state, which is the lowest for It is case 2. On the other hand, modes with a nozzle-shaped tube will significantly increase the friction

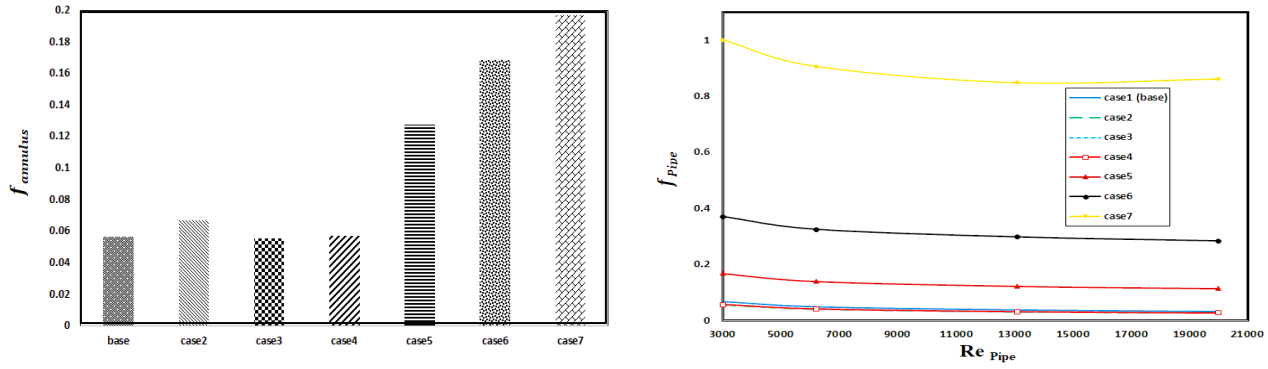

a b

Fig. 17: The friction coefficient in the outer pipe (a) and the inner tube for different (b) for different geometric cases

coefficient and consequently the fluid pumping power due to the huge increase in the flow speed, especially in the exit sections.

CONCLUSION

In this research, an attempt has been made to study the effect of geometrical changes in the inner tube of a double-tube heat exchanger. For this purpose, changes have been made in the geometric shape of the inner tube, which in the basic model is cylindrical with a circular section. In cases 2 to 4, flat tube shapes with different aspect ratios of 0.58, 0.44 and 0.3 are used, and in cases, 5 to 7, a convergent shape (nozzle-like) is used for the inner tube. has been The difference between cases 5 to 7 is in the diameter of the inner tube outlet, which is 20 mm, 16 mm and 12 mm for cases 5 to 7, respectively. It should be noted that the geometric shape of the outer tube and its dimensions as well as the mass flow rate of the cold fluid in the outer tube are considered constant in this. The most important goal of this research is to investigate the effects of these geometric changes on the thermal and fluid performance of the two-tube heat exchanger. In summary, the results of the present work are as follows:

- In all cases 2 to 7, and especially inside the inner tube, an increase in flow speed can be seen compared to the base case, and the highest speed is related to Case 2 of the flat inner tube states. In nozzle tube cases like this, the increase in speed is greater than in other cases. A slight drop in speed is observed in the outer tube.
- The pressure drop will also increase with the reduction of the inlet cross-section. In the case of the flat inner tube, Case 2 has the highest pressure drop and in the case of the inner tube of the nozzle, Case 7 has the highest pressure drop.
- At Reynolds numbers lower than 6000, the total pressure drop is generally different. In this period, as can be seen, the pressure drop in all cases with a flat inner tube is lower than the base case, which is the lowest pressure drop for Case 3.
- In the cases of the flat inner tube, the temperature in the inner tube at the end of the tube has dropped more than in the base case. The highest amount of heat transfer in Case 2.
- As a general conclusion, it can be stated that all the designs related to the nozzle-shaped inner tube (cases 5 to 7) show a weaker thermal and hydrodynamic performance compared to the base case in almost all studied Reynolds numbers. give But this case is slightly different from the cases with the flat inner tube. So that the thermal and fluid performance of these modes (modes 2 to 4) at low Reynolds numbers (up to 6000) is completely better than the basic model, which in total is the best performance in all aspects belonging to Case 4. But in Reynolds numbers higher than 6000, it is recommended to use the basic mode in general, due to the production problems of the inner tube.
- Therefore, in industries where the Reynolds number is below 6000 for the flow inside the inner pipe, it is cost-effective to use a flat pipe with geometric specifications of Case 4 with an aspect ratio of 0.3.

In future works, we will focus to study the exergy analysis [13, 21] of the results achieved in the present paper and set up an experimental model of case 4 which has the best performance in the Reynolds under 6000.

Received : Jul. 20, 2022 ; Accepted : Nov. 21, 2022

REFERENCES

[1] Omidi M., Farhadi M., Jafari M., A Comprehensive Review on Double Pipe Heat Exchangers, *Applied Thermal Engineering*, **110**: 1075-1090 (2017).

[2] Mehrabian M., Mansouri S., Sheykhzadeh G.A., The Overall Heat Transfer Characteristics of a Double Pipe Heat Exchanger: Comparison of Experimental Data with Predictions of Standard Correlations, *IJE Transactions B: Applications*, 395-409 (2002).

[3] Liao Q., Xin M., Augmentation of Convective Heat Transfer Inside Tubes with Three-Dimensional Internal Extended Surfaces and Twisted-Tape Inserts, *Chemical Engineering Journal*, **78(2-3)**: 95-105 (2000).

[4] Chen J., Müller-Steinhagen H., Duffy G.G., Heat Transfer Enhancement in Dimpled Tubes, *Applied thermal engineering*, **21(5)**: 535-547 (2001).

[5] Eiamsa-ard S., Thianpong C., Eiamsa-ard P., Turbulent Heat Transfer Enhancement by Counter/Co-Swirling Flow in a Tube Fitted with Twin Twisted Tapes, *Experimental Thermal and Fluid Science*, **34(1)**: 53-62 (2010).

[6] Nagarani N., K Mayilsamy., Experimental Heat Transfer Analysis on Annular Circular and Elliptical Fins, *International Journal of Engineering Science and Technology*, **2(7)**: 2839-2845 (2010).

[7] Iqbal Z., Syed K., Ishaq M., Optimal Convective Heat Transfer in Double Pipe with Parabolic Fins, *International Journal of Heat and Mass Transfer*, **54(25-26)**: 5415-5426 (2011).

[8] Kannan M., et al., Experimental and Analytical Comparison of Heat Transfer in Double Pipe Heat Exchanger, *International Journal of Automobile Engineering Research and Development*, **3**: 1-10 (2012).

[9] Zhang L., et al., Fluid Flow Characteristics for Shell Side of Double-Pipe Heat Exchanger with Helical Fins and Pin Fins, *Experimental Thermal and Fluid Science*, **36**: 30-43 (2012).

[10] Bhuiya M., et al., Heat Transfer and Friction Factor Characteristics in Turbulent Flow through a Tube Fitted with Perforated Twisted Tape Inserts, *International Communications in Heat and Mass Transfer*, **46**: 49-57 (2013).

[11] Totala N., et al., Manufacturing and Comparative Analysis of Threaded Tube Heat Exchanger with Straight Tube Heat Exchanger, *Int. J. Eng .Sci.*, **4(7)**: 77-85 (2014).

[12] Karanth V.K., Murthy K., Numerical Study of Heat Transfer in a Finned Double Pipe Heat Exchanger, *World Journal of Modelling and Simulation*, **11(1)**: 43-54 (2015).

[13] Rostami S., Ahmadi N., Khorasani S., Experimental Investigations of Thermo-Exergitic Behavior of a Four-Start Helically Corrugated Heat Exchanger with Air/Water Two-Phase Flow, *International Journal of Thermal Sciences*, **145**: 106030 (2019).

[14] Dizaji H.S., Jafarmadar S., Mobadersani F., Experimental Studies on Heat Transfer and Pressure Drop Characteristics for New Arrangements of Corrugated Tubes in a Double Pipe Heat Exchanger, *International Journal of Thermal Sciences*,. **96**: 211-220 (2015).

[15] Huu-Quan D., et al., 3D Numerical Investigation of Turbulent Forced Convection in a Double-Pipe Heat Exchanger with Flat Inner Pipe, *Applied Thermal Engineering*, **182**: 116106 (2021).

[16] Swamee P.K., Aggarwal N., Aggarwal V., Optimum Design of Double Pipe Heat Exchanger, *International Journal of Heat and Mass Transfer*, **51(9-10)**: 2260-2266 (2008).

[17] Petukhov B.S., Heat Transfer and Friction in Turbulent Pipe Flow with Variable Physical Properties, in "Advances in Heat Transfer", Elsevier, 503-564 (1970).

[18] Patankar S.V., "Numerical Heat Transfer and Fluid Flow", CRC Press (2018).

[19] Norouzi N., Shiva N., Khajehpour H., Optimization of Energy Consumption in the Process of Dehumidification of Natural Gas, *Biointerface Research in Applied Chemistry*, **11**: 14634-14639 (2021).

[20] Samanipour H., et al. The Study of Cylindrical Polymer Fuel Cell's Performance and the Investigation of Gradual Geometry Changes' Effect on Its Performance, *Periodica Polytechnica Chemical Engineering*, **6(3)**: 513-526 (2019).

[21] Norouzi N., Talebi S., Exergy, Economical and Environmental Analysis of a Natural Gas Direct Chemical Looping Carbon Capture and Formic Acid-Based Hydrogen Storage System, *Iranian Journal of Chemistry and Chemical Engineering (IJCCE)*, **41(4)**: 1436-1457 (2021).